AJDS LAZHAR Al-Azhar Journal of Dental Science
Vol. 27- No. 3- 367:377- July 2024
Print ISSN 1110-6751 | online ISSN 2682 - 3314
https://ajdsm.journals.ekb.eg
Oral Biology, Medicine & Surgical Sciences Issue *(Oral Biology, Oral Pathology, Oral Periodontology, Medicine, Oral & Maxillofacial Surgery)*

TUMOUR VOLUME AND S-PHASE FRACTION ANALYSIS IN INDUCED HAMSTER BUCCAL POUCH CARCINOMA UTILIZING CETUXIMAB IMMUNOTHERAPY

Ashraf Yehia Shamia[1*], Ahmed Abd-Alshakor Abd-Alhafez[2], Emad Soliman[2], Mohamed Gomaa Attia Zouair[3]

ABSTRACT

Objective: This study aimed to investigate tumor volume and synthesis phase fraction (SPF) analysis after cetuximab treatment on induced hamster buccal pouch (HBP) carcinoma. **Subjects and Methods:** 40 male Syrian hamsters were divided into 4 groups (G(s)) of 10. GI untreated animals served as negative controls. The right pouches of GII-GIV animals were painted with 7,12-dimethylbenz (a) anthracene (DMBA) 3 times a week for 14 weeks (ws). While GII received no extra treatment, GIII and GIV received cetuximab intraperitoneally (IP) 3 times a week for 3 ws, and for 6 ws respectively. Gross observations and tumor volume (TV) calculation were obtained after the end experiment. Fresh HBP specimens were surgically bisected into two sections, one for hematoxylin and eosin (H&E) to investigate the depth of invasion (DOI) and the other for immunohistochemistry (IHC) employing monoclonal antibody against epidermal growth factor receptor (EGFR). The other piece was employed for flow cytometry (FCM). Then statistical analysis was imploded. **Results:** TV, DOI, EGFR, and SPF aneuploid were highly significantly different between GII and GIV ($p = 0.001$), while SPF diploid recorded non-significant difference ($p>0.608$). **Conclusion:** The results of the present study indicated that the tumor volume and SPF is a powerful key indicator for tumor activity after treatment of HBP carcinoma by cetuximab.

KEY WORDS: HBP carcinoma, SPF, EGFR and cetuximab

INTRODUCTION

Resembling to oral squamous cell carcinoma (OSCC), DMBA-induced induced hamster buccal pouch (HBP) carcinoma was realized[1-3]. There has also been interest in the depth of invasion (DOI) in early-stage OSCC as a predictor of cervical nodal metastasis and local recurrence[4]. Most of these are caused by problems with how well treatments work, how far they spread, and how resistant the disease is[3, 5]. The behavior of tumors is also linked to the synthesis phase fraction (SPF), most of the time, tumors with a high SPF act more aggressively and have a worse prognosis[6].

The SPF test is easy to do on both fresh and formalin-fixed tissue samples, and it has become a useful diagnostic and prognostic tool for solid

1. Assistant Lecturer, Oral and Dental Pathology Department, Faculty of Dental Medicine, Al-Azhar University, Palestine
2. Lecturer, Oral and Dental Pathology Department, Faculty of Dental Medicine (Boys- Cairo), Al-Azhar University, Egypt.
3. Professor, Oral and Dental Pathology Department, Faculty of Dental Medicine (Boys-Cairo), Al-Azhar University, Egypt

• ***Corresponding author*:** dr_shamia@hotmail.com

DOI: *10.21608/AJDSM.2022.151452.1352*

malignant tumors in general and for oral cancer in particular[7]. There has been some disagreement about how to treat OSCC, but there is a lot of interest in chemotherapeutic treatments with cetuximab, carboplatin, and paclitaxel[8,9]. On top of that, cetuximab made several chemotherapeutic drugs work better against tumors in mouse xenograft models [10].

Cetuximab is a chimeric immunoglobulin G (IgG)-subclass monoclonal antibody that binds to the extracellular domain of the epidermal growth factor receptor (EGFR) with higher affinity than the natural ligands EGF, blocking the activation of its intracellular domain and the resulting tyrosine kinase-dependent signal transduction pathway[11], cetuximab also makes EGFR internalize[12], which has been used as a well-known and accepted experimental model for a number of studies, including biochemical, histological, immunohistochemistry (IHC), and molecular changes[13,14]. EGFR is a transmembrane glycoprotein that controls cell growth and division. It is a member of the tyrosine kinase growth factor receptor family[15].

There is more and more evidence that this receptor is overexpressed in up to 90% of HNSCC and is linked to a shorter chance of survival, which has led to research into drugs that target the EGFR pathway[16]. Thus, the primary aim of this study was to determine the therapeutic efficacy cetuximab as an anticancer therapy strategy in DMBA-induced HBP carcinoma, as well as the associated adverse events. The evaluation depends on the histological tumor tissue changes, IHC examination, and flow cytometry (FCM) studies.

SUBJECTS AND METHODS

Chemicals

Sigma-Aldrich provided the DMBA (0.5 percent), which was then dissolved in paraffin oil. phosphate-buffered saline (PBS) buffer (pH 7.4) was redispersed with cetuximab (C225, Erbitux Merck Serrano - Germany) and stored at 4°C until needed.

Animals

There are 40 male Syrian hamsters aged 5 weeks and weighing between 80 and 120 g. The hamsters were housed in common boxes with sawdust bedding in a controlled environment with humidity levels of 30-40%, temperature ranges of 20±2°C, and 12-hour light/12-hour dark cycles. A healthy hamster has a smooth, regular movement, bright, untroubled eyes, smooth, bright skin, and no parasites, sores, dry spots, or swellings on its coat.

Experimental design

After a week of adaptation, the animals were divided into 4 groups (G(s)). Each group consisted 10 animals. The right pouches of the animals in groups GII, GIII, and GIV were painted 3 times a week for 14 weeks with 0.5% DMBA in liquid paraffin to use a number 4 camel hairbrush**,** whereas the animals in group GI (negative control) were still not treated. The animals in GII (positive control) received no more medication, while those in GIII (cetuximab-3w) were injected intraperitoneally (IP) with 1 mg/animal of cetuximab at 3-day intervals for 3 ws and those in GIV (cetuximab-6w) were injected IP with 1 mg/animal of cetuximab at 3-day intervals for 6 ws [17].

General health examinations

The alterations in the animal's general health were monitored throughout the experiment. Hamsters that demonstrated any of the following signs (crowding in sneezing, anorexia, silence, corner, diarrhea, discharge from the nose or eyes, dampness around the tail, wheezing, and hair loss) of illness or disease were adapted.

Tumor volume measurement:

After termination of the experiment, gross observations of HBP mucosa were recorded (mucosal thickness, exudation, ulcers, and tumors). Then, the animals were euthanized, the right cheek pouch everted, and the diameter of each tumor was measured with a Vernier calliper. The tumor volume,

where the three diameters (mm) of the tumor are D1, D2 and D3, was calculated by the formula, Vmm3 = (4/3) π [(D1/2) (D2/2) (D3/2).

Sample collection and preparation

Right cheek pouch was cut in half and removed. One sample of fresh tissue was preserved in 10% neutral buffered formalin, handled normally, and fixed in paraffin blocks for histological analysis. The other fresh tissue sample underwent mechanical digestion, immobilized, and FCM examination.

Histopathological examinations

Utilizing a rotary microtome, 4μm thick tissue sections were cut from paraffin blocks, processed, mounted on glass slides, and stained with Hematoxylin and Eosin (H&E) for light microscopic inspection.

Measurement of the invasion's depth (DOI)

The H&E slide was used to calculate the DOI of each surgical specimen. From the base layer of the surface epithelium to the deepest site of tumor infiltration, the DOI was estimated. The American Joint Committee on Cancer (AJCC) classifies it further as less invasive at 5 mm, moderately invasive at 6–10 mm, and extremely invasive at 10 mm. The Leica QWIN V3 image analyzer computer system (Switzerland), which was run using the Leica QWIN V3 software, calculated the DOI. This was carried out in the Faculty of Dental Medicine (Boys-Cairo), Oral and Dental Pathology Department of Al-Azhar University, Egypt.

Immunohistochemical examination:

Other tissue sections 4 μm were placed on positively charged slides. The sections were deparaffinized in xylene and rehydrated via graded ethanol (100%, 95% and 70%), each run for 5 minutes. The slides were then rinsed in distilled water and PBS, each for 5 minutes. The sections were enzymatic cells treated by immersion in the slide racks container with 0.1% of pepsin, prepared one hour early (Pepsin: 0.2g, Calcium chloride: 0.2g and distilled water: 200 ml), then immersed in a water bath for 30 minutes at 37˚C in the hot oven, as enzymatic retrieval methods.

Slides were then cleaned in PBS, each for 5 minutes. Endogenous peroxidase activity was inhibited for 10 minutes at room temperature using 3% solution of hydrogen peroxide in methanol. Then, the samples were rinsed twice with PBS, each for 5 minutes, pH 7.2 to 7.6. Then, excess liquid was blotted around the tissues with filter paper. A serum block was applied to cover the specimen. The slides were incubated for 10 minutes at room temperature. The solution was drained and did not rinse after this step.

To cover the tissue sections, two to three drops of the primary polyclonal IgG EGFR antibody at a dilution of 1:50 were applied. The slides were kept in the refrigerator overnight at 4°C. After that, the slides were rinsed in distilled water and then in PBS for 5 minutes. For 30 minutes at room temperature, the slides were thoroughly covered with biotinylated (secondary antibody), ready to use. Excess fluid was wiped around the tissues with filter paper after washing the slides three times in PBS for five minutes. The slides were thoroughly covered with peroxidase-labeled streptavidin and left at room temperature for 30 minutes before being rinsed in PBS.

The tissue slices were dyed with DAB for 2 minutes before being immersed in cold water to cease the reaction. Mayer's hematoxylin was used to counterstain the tissue sections for 1 minute before rinsing in tap water. The slides were soaked in xylene after being immersed in two variables of 95% alcohol accompanied by two modifications of absolute alcohol, each for three minutes. Before mounting, three three-minute washes were allowed. Each slide was immersed in xylene for 1 second before being mounted with DPX and covered with coverslips. On immunostained tissue sections, the proportion of positive cases and the localization of immunostaining within the tissues were analyzed using a light microscope. Furthermore, the percentage of EGFR-positive cells with

immunostaining surface area was calculated using an image analysis computer system.

Cancer cell DNA cell cycle analysis:

Tumor tissue from each animal was cut into 3 sections of 50 μm thickness and transferred for DNA cytometric analysis of DNA ploidy and SPF in the Flow Cytometry Unit, Clinical Pathology Department, South Egypt Cancer Institute. Single nuclear suspensions were prepared by filtering through a 50 μm nylon mesh. Sample with the stained nuclei were analyzed using a and FACSCaliber FCM (Becton Dickinson Biosciences, San Jose, California USA).

Cell fit software was used to acquire and analyze the obtained data. The fluorescence signals from at least 50.000 nuclei were plotted and displayed as a frequency histogram. The SPF were taken as flow cytometric variables. The percentages of the cell cycle phase as well as the DNA indices of the aneuploid clones were calculated using the mod-fit software package. The SPF was estimated as percentage of cells occupying the region between the mean channel number for G0/G1 and that of G2/M. The cut off for the SPF was set as the mean ±2 standard deviation (SD) and considered as either being low or high.

Interpretation of DNA:

The X-axis shows the intensity of fluorescence of propidium iodide attached to DNA, while the Y-axis represents the number of events (cells or nuclei). DNA diploid tumors were defined as those having a single G0/G1 peak and a DI of 0.95 to 1.05 to the reference sample. The tumors were categorized as DNA aneuploid if two separate G0/G1 peaks were found, with an aberrant G0/G1 peak accounting for at least 15% of the total occurrences and a corresponding G2/M peak. By dividing the aberrant (aneuploid) G0/G1 peak by the mean channel number of the normal (diploid) G0/G1 peak, the relative DNA content was estimated. The abbreviation DI stands for the ratio. A sample with a DI of less than 0.95 (Hypodiplod) or more than 1.05 was considered aneuploid (Hyperdiploid). The DI was assessed by a machine and estimated using statistical techniques**.**

Statistical analysis

The mean and standard deviation were computed after statistical analysis of the data (SD). Using SPSS version 17.0 for Windows, a one-way analysis of variance was carried out (ANOVA). ANOVA was used with quantitative data and parametric distribution, together with post hoc analysis using the LSD test, to distinguish between more than two distinct groups. The following p-values were used to determine significance: p 0.05 for significant, p > 0.05 for non-significant, and p 0.001 for highly significant.

RESULTS

Gross observations and tumors volume:

GI examination revealed no obvious alterations, neither hair loss or skin ulcerations. The HBP was normal pale pink with no pathological or inflammatory signs, their buccal pouch length was from (5-5.5) cm **(Fig. 1A).** Those in **GII**, all hamsters demonstrated debilitation and observable hair loss with para-oral skin ulcerations. Large exophytic growths with prominent vascularity in the animals' pouches, in addition to eroded, and ulcerative areas with spontaneous bleeding were seen **(Fig. 1B).** The mean tumors volume measurement of tumor-bearing animals in 10 animals in **GII** was 814.6 mm3 (620 – 1005 mm3), and the pouch length in **GII** recorded from (1.5-2 cm). The mean tumors volume measurement in those of **GIII** and **GIV** was 269.13 mm3 (230.4 – 310.2 mm3) and 247.18 mm3 (180.1 – 390.5 mm3), respectively. The pouch length in **GIII** recorded from 3-3.5cm **(Fig. 1C)** and in **GIV** was 3.5-4cm **(Fig. 1D).** Comparing the **GII** with the various treated groups **GIII** and **GIV** according to tumor volume, there was highly significant difference (p value < 0.001). Contrarily, there was a non-significant difference between **GIII** and **GIV** (p-value = 0.728).

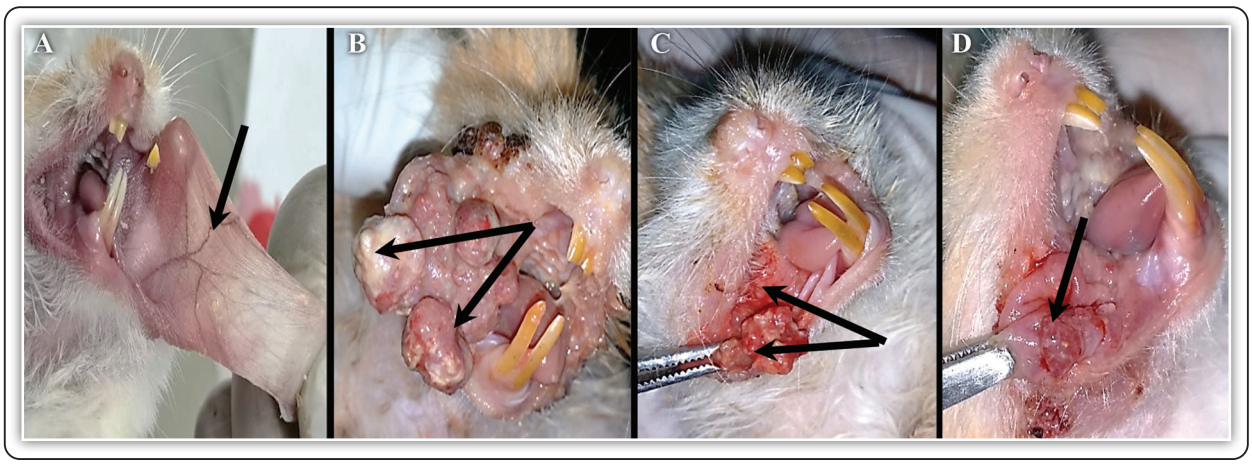

FIG (1) GI's HBP reveals normal buccal pouch mucosa, which had a smooth, pink appearance **1A.** GI's HBP indicates normal buccal pouch mucosa, which appeared pink in color with a smooth surface (arrow). **1B.** GII's HBP demonstrates multiple exophytic papillary tumor masses surrounded by bleeding areas (arrows). **1C**. GIII's HBP demonstrates medium size nodule with bleeding areas (arrows). **1D**. GIV's HBP indicates a small size nodule with little bleeding areas (arrows).

Histological findings:

The **GI** exhibited a normal thin stratified squamous epithelium with minor keratinization, consisting of 2-3 layers of squamous cells. A subepithelial connective tissue and a muscle layer were discovered **(Fig. 2A). GII:** The overlying epithelium revealed multiple areas with dysplastic feature including basilar hyperplasia, hyperchromatism, loss of polarity, large nucleoli, altered N/C ratio, and cellular and nuclear pleomorphism **(Fig. 2B).** Destructive basement membrane with invasive epithelial islands into the underlying connective tissue. The mean DOI revealed 10.5mm. **GIII:** In 2 hamsters out of 10 had epithelial dysplasia with top-to-bottom changes or carcinoma in situ. In contrast, the other eight had well-differentiated SCC that had not progressed to deeper parts. Distal necrosis was reduced, inflammatory infiltration was increased, and collagen fibers were increased **(Fig. 2C). GIV:** In three hamsters out of 10, exhibited epithelial dysplasia (hyperchromatism, changed N/C ratio, conspicuous nucleoli, cellular & nuclear pleomorphism, and numerous group cell keratinization).

In comparison, the remaining seven hamsters exhibited well-differentiated SCC that did not extend to the deeper connective tissue, the connective tissue exhibited a reduction in distal necrosis, an elevation in inflammatory infiltration, and an elevation in the thickness of the striated muscle layer. At the same time, a few tumor masses were substituted by proliferating fibrous tissue with enhanced collagen deposition **(Fig. 2D).** The mean DOI in GIII and GIV revealed 3.5mm & 2.4mm respectively. There was highly significant difference between treated groups (GIII and GIV) and positive control group (GII) (p value < 0.001). Furthermore, there was significant difference between GIII and GIV. (p value < 0.012).

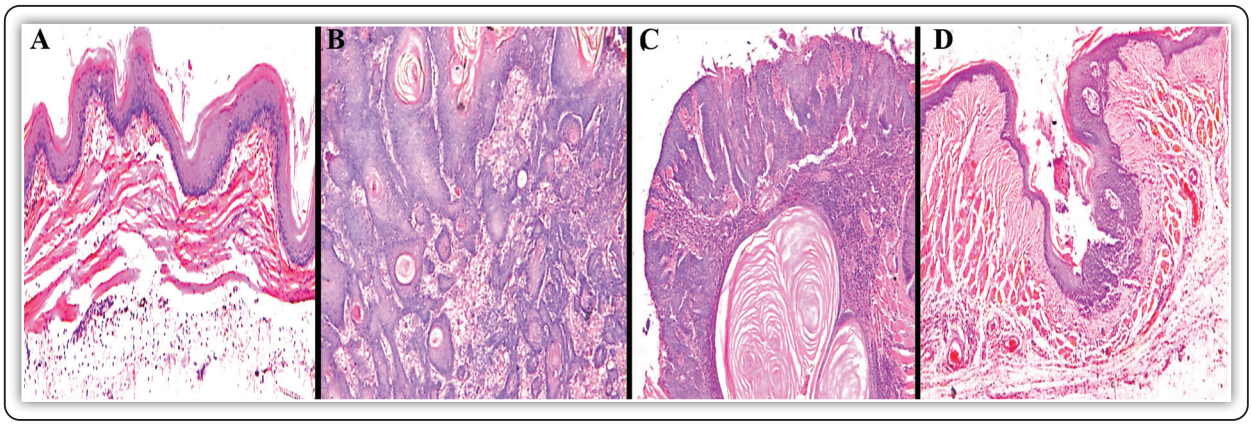

FIG (2) **GI** H&E stain demonstrates two to four layers of epithelium, superficial keratinized squamous cells, connective tissue layer, flattened rete ridges, muscular layer, and deep layer of loose areolar connective tissue. **2B. GII** H&E stain shows well-differentiated SCC with deep penetration of several tumor islands into the underlying connective tissue and sub-epithelial inflammatory infiltrates. **2C. GIII** H&E stain reveals well differentiated SCC (superficial invasion). **2D. GIV** H&E stain shows extensive dysplasia with hyperkeratosis.

Immunohistochemical findings

GI: The IHC staining using EGFR antibody exhibited positive cytoplasmic and membranous expression, which was limited to basal and keratinous layers **(Fig. 3A).** (mean = 8.2%). **GII:** The IHC positive staining in the central part of both well-differentiated and moderately differentiated SCC. While the Peripheral cells of the invasive nests exhibited negative staining for EGFR **(Fig. 3B).** (mean =53.4%). **GIII:** The IHC positive staining throughout the overlying epithelium, and the central part of the invasive nests of well-differentiated SCC, with negative staining of Peripheral cells of the invasive nests **(Fig. 3C).** (mean =45.9%). **GIV:** The IHC positive staining throughout the overlying epithelium, as well as in the central part of the invasive nests of well-differentiated SCC. Peripheral cells of the invasive nests exhibited negative staining for EGFR **(Fig. 3D).** (mean=32.5%). There was highly significant difference between both GI and GII, also between GII and GIV (p-value<0.001). There was a significant difference between GII & GIII (p-value=0.002). Moreover, there was non-significant difference between GIII and GIV (p-value = 0.143) **(Fig. 4).**

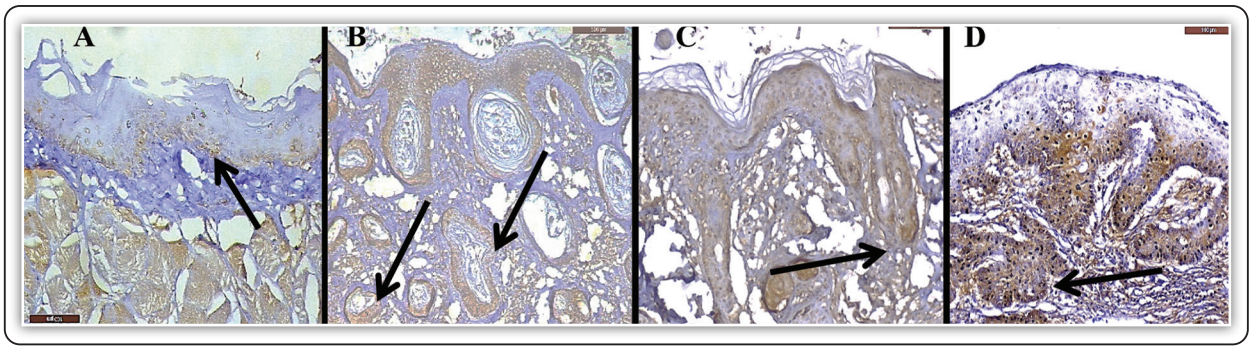

FIG (3) **A.** IHC expression of **GI** shows negative staining throughout the epithelial layers, except for positive cytoplasmic and membranous reactivity of some cells of the basal cell layer, and keratinous layer. Connective tissue shows a nonspecific reaction. 3**B**. EGFR expression of **GII** indicates positive cytoplasmic and membranous staining via the overlying epithelium, as well as in the invasive nests**(arrow)**. 3**C**. EGFR expression of **GIII** indicates positive cytoplasmic and membranous staining via the overlying epithelium, as well as in the invasive nests. 3`**D**. EGFR IHC expression of **GIV** demonstrates positive cytoplasmic and membranous staining via the overlying epithelium, as well as in the invasive nests.

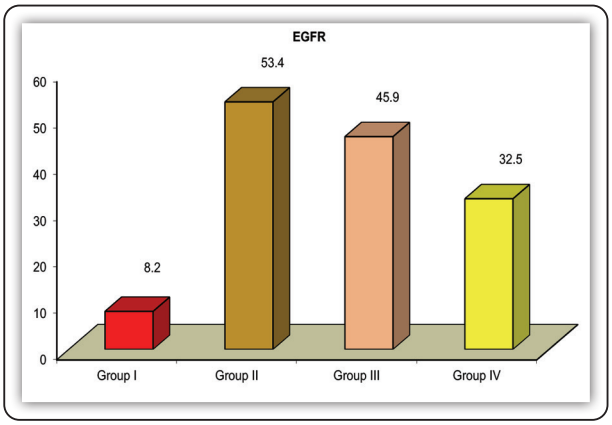

FIG (4) Comparison between the studied groups EGER

Detection of SPF analysis for cancer cells by FCM

The SPF values calculated for the cell cycles of the diploid **GI** ranged between 1.23% and 3.47% with a mean of 2.30%. In **GII**, SPF values ranged between 11.57% and 19.94% with a mean of 15.10% in diploid lesions, While the SPF diploid in those of **GIII and GIV** was ranged between 9.1% and 22.2% with a mean of 15.30 % and 10.7% and 21.7%, with a mean of 14.40 %, respectively.

The SPF values of the aneuploid lesions **GI** ranged between 1.2% and 3.4% with a mean of 2.30%. In **GII**, SPF values ranged between 22.7% and 30.1% with a mean of 26.60% in aneuploid lesions, While the SPF aneuploid in those of **GIII and GIV** was ranged between 8.9% and 23.1% with a mean of 16.80 % and 13.6% and 31.1%, with a mean of 19.70 %, respectively.

Comparing the control groups (GI and GII), there was highly significant difference (p value <0.001) regarding to SPF (diploid and aneuploid). Comparing positive control group GII with the various treated Gs GIII and GIV according to SPF diploid, there was non-significant difference (p value <0.883), (p value <0.608), respectively. Contrarily, according to SPF aneuploid there was highly significant difference (p value <0.000). Comparing the treated Gs (GIII and GIV), there was non- significant difference regarding to either SPF diploid (p value <0.509) or SPF aneuploid (p value <0.184).

DISCUSSION

One of the most disfiguring kinds of cancer is oral cancer. Despite advances in oral cancer treatment strategy, it continues to be a major cause of morbidity in human populations. The oral carcinogenesis model's hamster cheek pouch system is useful for gaining a better understanding of cancer biology, prevention, and treatment. Tumor volume, H&E stain, IHC staining with EGFR antibody, and SPF analysis for cancer cells by FCM evaluation all revealed different insights.

In the present study, compared to GI, GII revealed noticeable systemic debilitation in all animals, in addition to perioral alteration and HBP tumor growth. The latter was distinguishable by the results of the volume of tumor-bearing pattern (620 – 1005 mm3). Also, a decrease in the pouch length in GII (1.5-2 cm) compared to that of GI (5 cm) due to necrosis in the distal end of the pouch. Generally speaking, The results in GII are in consistence with those reported by other investigators [18].These observations are mainly due to the strong toxic DMBA effect[19].

In the present study, both GIII and GIV showed a relatively slight improvement in the animal's general health. The pouch length was increased in GIII (2.5-3cm) and in GIV (3-3.5cm) compared to GII (1.5-2cm), this is due to marked decrease of distal necrosis and inflammatory infiltration. Furthermore, the mean tumors volume GII (620- 1005 mm3), compared to GIII and GIV was decreased (230.4 – 310.2 mm3) and (180.1 – 390.5 mm3), respectively with highly significant difference (p value < 0.001). Contrarily, there was a non-significant difference between GIII and GIV (p-value = 0.728). These results were in line with other study[20]. The non-responsiveness of cetuximab as a single agent may be caused by multiple intrinsic and extrinsic/ acquired resistance mechanisms. In the case of OSCC, many tumors remain non-responsive to cetuximab in which the single-agent response rate of this drug is less than 15%. Nevertheless,

cetuximab is known to provide a clinical benefit when used either in conjunction with radiation or in combination with chemotherapy[21]. From a clinical point of view, Lu et al. (2007)[22], reported that acquired resistance occurs after an initial response to therapy and eventually all OSCC patients will relapse or become insensitive to further cetuximab therapy.

In the present study, the histopathological findings, using H&E stain, GII revealed a development of diverse patterns of invasive SCC (50% well-differentiated and 50% moderately differentiated) that expanded into deeper areas of connective tissue (C.T) (DOI=10.5mm). These results in line with previous ones reported that 100% tumor growth occurred after 14 weeks of painting DMBA alone on the hamster's cheek pouches[19, 23]. This could be due to proclivity for carcinogenesis since it is metabolized by phase I enzymes such as cytochrome P450 to its final carcinogenic metabolite, dihydrodiol epoxide, which damages DNA, this in turn causing mutation and cancer[24]. Furthermore, ROS has been implicated throughout phases of carcinogenesis (promotion, initiation, and progression). ROS can cause DNA damage, proto-oncogenes stimulation, tumor suppressor genes suppression, all of which can lead to neoplastic transformation[25]. Contrastingly, in the study conducted by Hussein et al (2018)[26], only 66.67% of the hamsters developed oral tumors, and that could be attributed to the different solvent material.

The histopathological findings in GIII and GIV displayed that 90% of the hamsters have less invasive well-defined SCC without spread to deeper areas, DOI in GIII and GIV were 3.5 and 2.4mm, respectively. These results, compared to GII, reflected highly difference between (GIII and GII) and (GIV and GII) (p-value <0.001). They were in line with another study Boeckx et al (2013) [20].

In the present study, using IHC staining, GII reveled positive membranous-cytoplasmic expression of EGFR (53.4%) in contrast to GI that showed positive membranous-cytoplasmic expression (8.2%) with restriction to the basal and keratinous layer, this reflected by highly significant expression (p-value < 0.001). These findings agree with those of others[27, 28]. Numerous studies have indicated that when OSCC cells were compared to the normal epithelium, EGFR was overexpressed, which was assumed to have an effect on cell proliferation and survival in OSCC [28]. Detection of the EGFR extracellular domain revealed no clinical correlation. According to OSCC research, the EGFR-mediated PI3K/Akt/mTOR signaling pathway stimulates inflammation, proliferation, angiogenesis, and metastasis[29]. In summary, phosphorylated EGFR tyrosine residues activate downstream PI3K/Akt/mTOR signaling pathways, which control NF-ϰB activity in response to IϰBα kinase (IKK)-dependent IϰBα phosphorylation and degradation[30].

There was no difference in the area percentage of EGFR across different degrees of OSCC differentiation in our investigation, which is consistent with Ramu et al (2018) [31]. This finding may imply that the level of differentiation of malignant keratinocytes is unrelated to EGFR. Theocharis et al(2017)[32], believe that a modification in the regulation of cell proliferation is indicated by an elevation in the area percentage of EGFR, the number of cells damaged is the key sign of altered cell proliferation.

GIII and GIV revealed positive membranous-cytoplasmic expression of the EGFR (45.9% -42.4%) respectively, which was found in all over the epithelium and in the middle of well-differentiated SCC nests. These findings were realized by highly significant different either GII and GIII or GIV (p-value = 0.002), (p-value <0.000) respectively, this is in line with other studies [33, 34]. This could explain as cetuximab blocked the activity of EGFR in cells that had a lot of EGFR auto-phosphorylation at the start of the cell, even though the cells did not have a lot of EGFR expression. EGFR signaling

and how well EGFR suppression works are also based on other factors, like EGFR mutations and polymorphisms in the downstream pathways[34].

The SPF values in GII of the diploid lesions ranged between 1.93% and 25.94% with a mean of 15.10 %, and the SPF of the aneuploid lesions ranged between 10.25% and 51.50% with a mean of 26.60%. The difference in the SPF values of (diploid and aneuploid) was statistically significant (P-value < 0.05). The mean SPF in our study is consistent with the reported results for FCM determined SPF in HNC[35]. These results indicated that high SPF reflects the high proliferative activity of the tumor.

The SPF values in GIII and GIV for diploid (15.30% - 14.40%) respectively, while for aneuploid lesions SPF (16.80% - 19.70%) respectively. These findings according to SPF diploid reflected non-significant difference either in GII and GIII or GIV (p-value = 0.883 - 0.608) respectively. Contrastingly, findings according to SPF aneuploid reflected highly significant difference either in GII and GIII or GIV (p-value = 0.000). These findings corroborate those of Otsuka et al (2019) [36], who discovered that tumors with low aneuploidy scores contained considerably more immune cells positive for CD8, Foxp3, and PD-1. The existence of these inflammatory markers suggests that tumors with low levels of aneuploidy may be more immunogenic than cancers with high levels of aneuploidy, which may lead to enhanced responses to immune checkpoint suppression[37] . In contrast, author reported, that the SPF is significantly higher in aneuploid OSCC tumours than in diploid carcinomas and it is a better indicator of tumor aggressiveness and predicting disease prognosis than the DNA ploidy [38].

CONCLUSION

This study demonstrated cetuximab's time-dependent immunotherapeutic efficacy. 1 mg of cetuximab every 3 days for 6 weeks had a strikingly higher response rate than 3 weeks, as measured by tumor volume and SPF.

Institutional review board statement

The National Research Council's Guide for the Care and Use of Laboratory Animals have been followed. All experiments were approved by ethical committee of Faculty of Dental Medicine (Boys Cairo), Al-Azhar University, Egypt (Ethical Code No. 489/2302).

REFERENCES

1. Ma H, Liu C, Zhang S, Yuan W, Hu J, Huang D, et al. miR-328-3p promotes migration and invasion by targeting H2AFX in head and neck squamous cell carcinoma. Journal of Cancer. 2021;12(21):6519.
2. Zawam HH, Selim A, Osman NO, Edesa W. Factors Influencing the Response Rate and Survival of Testicular Germ Cell Tumors: A Single Institution Experience from Egypt. Research in Oncology. 2021;17(2):66-72.
3. Ghantous Y, Bahouth Z, El-Naaj IA. Clinical and genetic signatures of local recurrence in oral squamous cell carcinoma. Archives of oral biology. 2018;95:141-8.
4. Faisal M, Abu Bakar M, Sarwar A, Adeel M, Batool F, Malik KI, et al. Depth of invasion (DOI) as a predictor of cervical nodal metastasis and local recurrence in early stage squamous cell carcinoma of oral tongue (ESSCOT). 2018;13(8):e0202632.
5. Yanamoto S, Umeda M, Kioi M, Kirita T, Yamashita T, Hiratsuka H, et al. Multicenter retrospective study of cetuximab plus platinum-based chemotherapy for recurrent or metastatic oral squamous cell carcinoma. Cancer chemotherapy and pharmacology. 2018;81(3):549-54.
6. Driemel O, Maier H, Kraft K, Haase S, Hemmer JJOr. Flow cytometric DNA ploidy in salivary gland tumours. 2005;13(1):161-5.
7. Gupta N, Kumar RJJS. Role of flow cytometry in diagnostic pathology. 2010;12(3):110.
8. Enokida T, Ogawa T, Homma A, Okami K, Minami S, Nakanome A, et al. A multicenter phase II trial of paclitaxel, carboplatin, and cetuximab followed by chemoradiotherapy in patients with unresectable locally advanced squamous cell carcinoma of the head and neck. Cancer medicine. 2020;9(5):1671-82.
9. Peng W, de Bruijn HS, Ten Hagen TL, van Dam GM, Roodenburg JL, Berg K, et al. Targeted photodynamic therapy of human head and neck squamous cell carcinoma with anti-epidermal growth factor receptor antibody

cetuximab and photosensitizer ir700dx in the mouse skin-fold window chamber model. Photochemistry and Photobiology. 2020;96(3):708-17.

10. Bauman JE, Duvvuri U, Gooding WE, Rath TJ, Gross ND, Song J, et al. Randomized, placebo-controlled window trial of EGFR, Src, or combined blockade in head and neck cancer. 2017;2(6).
11. Gillison ML, Trotti AM, Harris J, Eisbruch A, Harari PM, Adelstein DJ, et al. Radiotherapy plus cetuximab or cisplatin in human papillomavirus-positive oropharyngeal cancer (NRG Oncology RTOG 1016): a randomised, multicentre, non-inferiority trial. 2019;393(10166):40-50.
12. Giordano G, Remo A, Porras A, Pancione MJC. Immune resistance and EGFR antagonists in colorectal cancer. 2019;11(8):1089.
13. Peng W, de Bruijn HS, Ten Hagen TL, van Dam GM, Roodenburg JL, Berg K, et al. Targeted photodynamic therapy of human head and neck squamous cell carcinoma with anti-epidermal growth factor receptor antibody cetuximab and photosensitizer ir700dx in the mouse skin-fold window chamber model. 2020;96(3):708-17.
14. Taberna M, Oliva M, Mesía R. Cetuximab-containing combinations in locally advanced and recurrent or metastatic head and neck squamous cell carcinoma. Frontiers in oncology. 2019;9:383.
15. Ang KK, Berkey BA, Tu X, Zhang H-Z, Katz R, Hammond EH, et al. Impact of epidermal growth factor receptor expression on survival and pattern of relapse in patients with advanced head and neck carcinoma. 2002;62(24):7350-6.
16. Gettinger SN, Horn L, Gandhi L, Spigel DR, Antonia SJ, Rizvi NA, et al. Overall survival and long-term safety of nivolumab (anti–programmed death 1 antibody, BMS-936558, ONO-4538) in patients with previously treated advanced non–small-cell lung cancer. Journal of clinical oncology. 2015;33(18):2004.
17. El-Mansy MN, Hassan MM, El-Nour A, Kholoud M, El-Hosary WH. Evaluation the safety of thymoquinone loaded on gold nanoparticles in the treatment of hamster buccal carcinogenesis. Suez Canal University Medical Journal. 2017;20(1):20-8.
18. Bruna F, Arango-Rodríguez M, Plaza A, Espinoza I, Conget P. The administration of multipotent stromal cells at precancerous stage precludes tumor growth and epithelial dedifferentiation of oral squamous cell carcinoma. Stem Cell Research. 2017;18:5-13.
19. El-Hossary WH, Hegazy E, El-Mansy MN. Topical Chemopreventive Effect Of Thymoquinone Versus Thymoquinone Loaded On Gold Nanoparticles On Dmba-Induced Hamster Buccal Pouch Carcinogenesis (Immunohistochemical Study). Egyptian Dental Journal. 2018;64(4-October (Oral Medicine, X-Ray, Oral Biology & Oral Pathology)):3523-33.
20. Boeckx C, Baay M, Wouters A, Specenier P, Vermorken JB, Peeters M, et al. Anti-epidermal growth factor receptor therapy in head and neck squamous cell carcinoma: focus on potential molecular mechanisms of drug resistance. The oncologist. 2013;18(7):850-64.
21. Mohammed ES, Ahmed MM, Zouair MGA. Synergistic effect between cetuximab and curcumin on experimentally induced hamster buccal pouch carcinoma. Al-Azhar Journal of Dental Science. 2017;20(2):145-52.
22. Lu Y, Li X, Liang K, Luwor R, Siddik ZH, Mills GB, et al. Epidermal growth factor receptor (EGFR) ubiquitination as a mechanism of acquired resistance escaping treatment by the anti-EGFR monoclonal antibody cetuximab. Cancer research. 2007;67(17):8240-7.
23. Swidan S, Hassan M, El-Hossary W. Chemopreventive effect of different doses of nanothymoquinone on chemically–induced oral carcinogenesis: Msc. Thesis., Suez Canal University; 2016.
24. Baldasquin-Caceres B, Gomez-Garcia F, López-Jornet P, Castillo-Sanchez J, Vicente-Ortega V. Chemopreventive potential of phenolic compounds in oral carcinogenesis. Archives of Oral Biology. 2014;59(10):1101-7.
25. Naveenkumar C, Raghunandhakumar S, Asokkumar S, Devaki T. Baicalein abrogates reactive oxygen species (ROS)-mediated mitochondrial dysfunction during experimental pulmonary carcinogenesis in vivo. Basic & clinical pharmacology & toxicology. 2013;112(4):270-81.
26. Hussein AM, El-Sheikh SM, Darwish ZE, Hussein KA, Gaafar AI. Effect of genistein and oxaliplatin on cancer stem cells in oral squamous cell carcinoma: an experimental study. Alexandria Dental Journal. 2018;43(1):117-23.
27. Rajeswari MRC, Saraswathi TR. Expression of epithelial growth factor receptor in oral epithelial dysplastic lesions. Journal of oral and maxillofacial pathology: JOMFP. 2012;16(2):183.
28. Haidar Z, Fernández A, Fernández J, Marshall M, Martínez R, Niklander S. Difference in EGFR expression and mean vascular density in normal oral mucosa, oral epithelial dysplasia and oral squamous cell carcinoma. Journal of Oral Research. 2017;6(2):39-45.

29. Hou X, Yang F, Liu W, Fu Z, Chen L, Li Z, et al. Signaling pathways that facili-tate chronic inflammation-induced carcinogenesis. J Cell Signal. 2015;1:9.

30. Freudlsperger C, Burnett JR, Friedman JA, Kannabiran VR, Chen Z, Van Waes C. EGFR–PI3K–AKT–mTOR signaling in head and neck squamous cell carcinomas: attractive targets for molecular-oriented therapy. Expert opinion on therapeutic targets. 2011;15(1):63-74.

31. Dragomir L, Mărgăritescu C, Florescu A, Olimid A, Dragomir M, Popescu MJRJME. The immunoexpression of EGFR and Her2/neu in oral squamous carcinoma. 2012;53(3):597-601.

32. Theocharis S, Giaginis C, Dana E, Thymara I, Rodriguez J, Patsouris E, et al. Phosphorylated epidermal growth factor receptor expression is associated with clinicopathologic parameters and patient survival in mobile tongue squamous cell carcinoma. Journal of Oral and Maxillofacial Surgery. 2017;75(3):632-40.

33. Yin P, Cui S, Liao X, Yao X. Galectin-3 blockade suppresses the growth of cetuximab-resistant human oral squamous cell carcinoma. Molecular medicine reports. 2021;24(4):1-9.

34. Kriegs M, Clauditz TS, Hoffer K, Bartels J, Buhs S, Gerull H, et al. Analyzing expression and phosphorylation of the EGF receptor in HNSCC. Scientific reports. 2019;9(1):1-8.

35. Oya R, Ikemura KJH, neck. Can flow cytometrically determined DNA ploidy and S-phase fraction predict regional metastasis in squamous cell carcinoma of the oral cavity? 2002;24(2):136-42.

36. Otsuka A, Dummer RG. New Therapies and Immunological Findings in Melanoma and Other Skin Cancers: Frontiers Media SA; 2019.

37. Badr El-Din NK, Ali DA, Alaa El-Dein M, Ghoneum M. Enhancing the apoptotic effect of a low dose of paclitaxel on tumor cells in mice by arabinoxylan rice bran (MGN-3/Biobran). Nutrition and cancer. 2016;68(6):1010-20.

38. Hussein AM, El-Sheikh SM, Attia MA, Ramadan OR, Omar EM, Gaber AHJEDJ. Analysis of DNA ploidy and S-phase fraction in relation to development of oral squamous cell carcinoma: an experimental study. 2019;65(3-July (Oral Medicine, X-Ray, Oral Biology & Oral Pathology)):2447-55.